PCCP

Accepted Manuscript

ROYAL SOCIETY OF CHEMISTRY

www.rsc.org/pccp

PCCP

ARTICLE

About the electronic and photophysical properties of Iridium (III)-pyrazino[2,3-f][1,10]-phenanthroline based complexes to use in electroluminescent devices†

Received 00th January 20xx,
Accepted 00th January 20xx

DOI: 10.1039/x0xx00000x

www.rsc.org/

Diego Cortés-Arriagada[a,*], Luis Sanhueza[b,*], Iván González[c], Paulina Dreyse[d] and Alejandro Toro-Labbé[a]

A family of cyclometalated Ir^{III} complexes was studied through quantum chemistry calculations to get insights into their applicability in light electrochemical cells (LECs). The complexes are described as $[Ir(R\text{-}C\^N)_2(ppl)]^+$, where ppl is the pyrazino[2,3-f][1,10]-phenanthroline ancillary ligand. The modification of the HOMO energy in all the complexes was achieved by means of different R-C^N cyclometalating ligands, with *R-ppy* (phenylpyridine), *R-pyz* (1-phenylpyrazole) or *R-pypy* (2,3'-bipyridine); in addition, inductive effects were taken into account by substitution with the *R* groups (*R* = H, F or CF_3). Then, compounds with HOMO-LUMO energy gaps from 2.76 to 3.54 eV were obtained, in addition to emission energies on the range of 438 to 597 nm. The emmision deactivation pathways confirm presence of metal-to-ligand transitions in all the complexes, which allow the strong spin orbit coupling effects, and then improving the luminiscent performance. However, the coupling with ligand and metal centered excited states was observed for the blue-shifted emitters, which could result in a decrease of the luminescent efficiencies. Furthermore, ionization potentials, electron affinities and reorganization energies (for hole and electron) were obtained to account for the injection and transport properties of all the complexes in electroluminescent devices.

Introduction

Organometallic and coordination complexes, including heavy metals such as ruthenium, rhenium, osmium and iridium have received a great attention due to their potential applications in photonic and optoelectronic materials[1-4]. This interest has been increased during the last two decades, particularly, with the use of Ir^{III} complexes of the type $Ir(C\^N)_3$ and $[Ir(C\^N)_2(N\^N)]^+$ (where C^N and N^N are the cyclometalating and ancillary ligands, respectively), involving large π-conjugated systems[5, 6]. Due to strong metal-induced spin orbit coupling (SOC) processes, these complexes populate the spin-forbidden triplet excited states to obtain high emission quantum yields[4, 7]. In addition, these compounds show different emission (and absorption) wavelengths, which are controlled by including different ligands in the molecular design[8]. According to this description, these complexes are used in solid state lighting systems such as organic light-emitting diodes (OLEDs) and light emitting electrochemical cells (LECs)[9-12]; moreover, the luminescent properties of Ir^{III} complexes turn them in efficient candidates for development of scintillating materials for radiation detection[13, 14]. In particular, LECs devices consist of a layer of an ionic transition metal complex (iTMC) with luminescent properties, sandwiched between two electrodes; a cathode consisting in a metal layer and a transparent conductive film (indium–tin oxide for example) that acts as anode. LECs have a simpler architecture than OLEDs, since the former are processed from solution, do not rely on air-sensitive metal electron injection layers, and hence they require less stringent packaging procedures. According to the description of the photophysical properties for cyclometalated Ir^{III} complexes, these compounds have been highlighted in the use of these devices[4, 9, 15-17].

The main electronic transitions involved in the optical properties of Ir^{III}-iTMCs, are metal-to-ligand (MLCT) and ligand-to-ligand (LLCT, electron promotions from the phenyl groups of the C^N to the N^N ligand) charge-transfer transitions, which are readily modulated by incorporation of electron-withdrawing/donating groups on these ligands[7]. In general, the N^N ligand can be modified with the purpose of stabilizing or destabilizing mainly the LUMO (lowest unoccupied molecular orbital), changing the HOMO–LUMO energy gap (HL_{gap}) and therefore the emission energy. For example, the use of N^N

[a] Nucleus Millennium Chemical Processes and Catalysis; Laboratorio de Química Teórica Computacional (QTC), Facultad de Química, Pontificia Universidad Católica de Chile, Av. Vicuña Mackenna 4860, Macul, Santiago, Chile. *Email: dcortesr@uc.cl
[b] Instituto de Ciencias Químicas, Facultad de Ciencias, Universidad Austral de Chile, Casilla 567, Valdivia, Chile. *Email: luis.sanhueza.vega@gmail.com
[c] Departamento de Química Inorgánica. Pontificia Universidad Católica de Chile, Av. Vicuña Mackenna 4860, Macul, Santiago, Chile. Vicuña Mackenna 4860, Macul, Santiago, Chile.
[d] Departamento de Química, Universidad Técnica Federico Santa María, Av. España 1680, Valparaíso, Chile.
†Electronic Supplementary Information (ESI) available: See DOI: 10.1039/x0xx00000x

ligands (combining high rigidity and electron delocalization) affect in the stabilization of LUMO orbital, due to increase of the acceptor π* character[18-20]. Alternatively, electron-withdrawing substituents in the C^N ligand decreases the electronic density of the metal, producing a higher stabilization of the HOMO (highest occupied molecular orbital). This effect has been achieved, for example, by incorporation of fluorine substituents in the phenyl ring of cyclometalating phenylpyridine ligands[4, 5, 21].

Focusing on the developing, synthesis and experimental implementation of cyclometalated metal complexes to their use in energy conversion devices, in this report, we account for the potential electroluminescent properties of nine cationic Ir^{III} complexes (Fig. 1), with variable cyclometalating ligand, to be implemented in LEC devices. The complexes studied are of the type $[Ir(R\text{-}C^N)_2(ppl)]^+$, where ppl is pyrazino[2,3-f][1,10]phenanthroline ligand. This ancillary ligand was selected looking for rigidity and high electron delocalization of its planar aromatic structure. We tailored the electronic properties of the Ir^{III}-ppl complexes using three different cyclometalating ligands (Fig. 1): *H-ppy* (2-phenylpyridine), *H-pyz* (1-phenyl-1H-pyrazole), and *H-pypy* (2,3'-bipyridine). These three ligands show different acceptor characters, and they would serve to change the HOMO energy. This behavior supposes the modification of the absorption and emission energies, allowing the modulation of the emission color[22]. In addition, electron withdrawing effects were incorporated by means of *R* substitutions (Fig. 1) at the cyclometalating ligands (R = H, F, or CF_3), which are expected to behave as HOMO stabilizers. Complexes **1**, **2** and **4** have been reported in literature and they serve as a comparison for the obtained results[20, 23, 24]. Furthermore, electronic properties were studied to measure the hole and the electron transport ability of all the complexes in LEC devices.

Computational details

Density functional theory (DFT) calculations were performed in the Gaussian09 program[25] with the B3LYP functional[26]; the 6-31G(d,p)[27, 28] basis set was used for H, C, N, O and F atoms; the quasirelativistic pseudopotential and basis set LANL2DZ[29] was adopted for Ir. The B3LYP functional was tested with other DFT methods to reproduce absorption/emission energies of the complex **1**, showing the best agreement with the experimental data (see our benchmark in the ESI†); besides, the B3LYP functional has been widely proved in literature to give accurate results with respect to experimental molecular structures and photophysical parameters of cyclometalated Ir^{III} complexes[30-33], in addition to be used as protocol to obtain their emission energies and quantum yields[34]. Vibrational frequencies were obtained in order to insure that the optimized structures correspond to energy minima, obtaining only positive frequencies. Electronic open-shell states were computed with the unrestricted formalism (UB3LYP). At the time dependent DFT methodology (TD-DFT), first 50 and 20 singlet and triplet excited states were obtained, respectively. Solvent effects were included by the PCM method, with dichloromethane as solvent (CH_2Cl_2, ε = 8.93). Wavefunction analysis were performed in the Multiwfn code[35].

Results and discussion

Geometrical parameters of the ground states

The general sketch labeling of the atoms is presented in Fig. 1, and selected geometrical parameters for complexes **1**-**9** are listed in Table S1 in the ESI†. All the complexes exhibit a pseudo octahedral configuration and the calculated geometric parameters correlates well with a crystalline structure obtained for related complexes Ir^{III} complexes[33, 36-38]. The bond lengths and angles that involve the metal center appear in the range of: $d(Ir\text{-}C_1)$=[2.02-2.01]Å, $d(Ir\text{-}N_1)$=[2.08-2.06]Å, $d(Ir\text{-}N_3)$=[2.23-2.21]Å, $\angle C_1\text{-}Ir\text{-}N_1$=[80-79]°, $\angle N_3\text{-}Ir\text{-}N_4$=[76-75]°, $\angle N_1\text{-}Ir\text{-}N_2$=[173-172]°, $\angle C_1\text{-}Ir\text{-}N_4$=[173-172]°. The similar geometrical parameters between all the complexes indicate that differences between them are coming only from their different electronic structures as will be discussed below.

Frontier molecular orbitals in the ground state

The effect of the C^N ligand on the frontier molecular orbitals HOMO and LUMO was investigated. Fig. 2 depicts the energy diagram showing the HOMO and LUMO surfaces, and the HOMO-LUMO energy gap (HL_{gap}) of the complexes **1**-**9**. In all the cases, the HOMO is based on a mixture of π and d orbitals of the C^N ligand and the metal center, respectively; while the LUMO is coming from antibonding π* orbitals centered in the ancillary ligand (for detailed information, see Table S2 in the ESI†). The HOMO and LUMO energy levels are stabilized by the presence of fluorine atoms (with F and CF_3 substituents), with an enhancement of the HL_{gap} as will be mentioned.

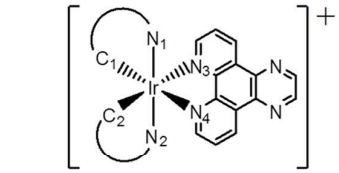

R	R - ppy	R - pyz	R - pypy
H	1	4	7
F	2	5	8
CF_3	3	6	9

Fig. 1 Schematic representation of the cyclometalated Iridium complexes studied in this work. Sketch labelling for the atoms coordinated to the metal center are included.

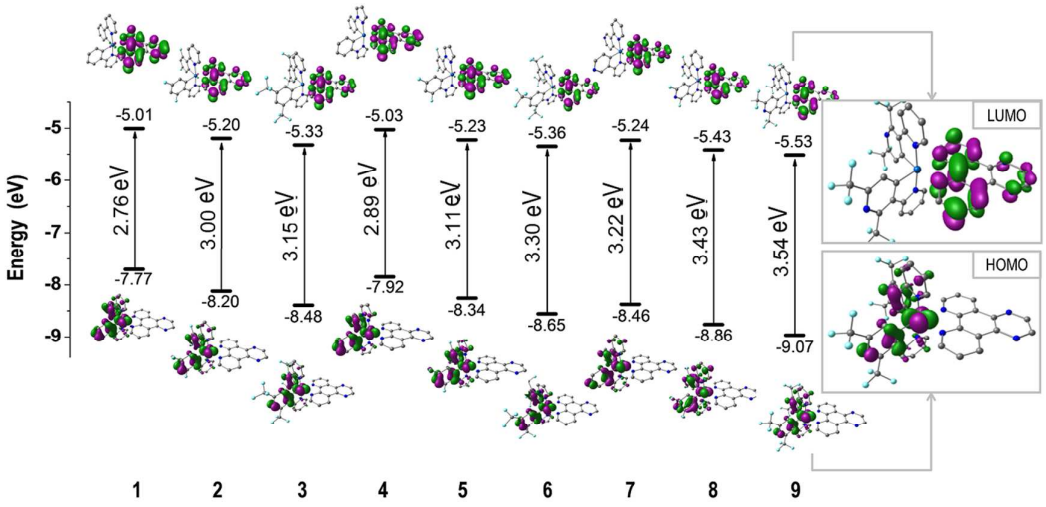

Fig. 2 Energy diagram and surfaces of the HOMO and LUMO for the systems **1**-**9**.

As noted above, in all cases the HOMO energy appears strongly influence and stabilized by the aromatic structure of the *C^N* ligand (*H-ppy, H-pyz or H-pypy*). For instance, the HOMO energy level of the complexes **4** and **7** is stabilized by 0.15 and 0.69 eV, respectively, with respect to the HOMO level of **1**, which is in agreement with the tendency of the oxidation potentials from cyclic voltametry measurements[39]. The same tendency is observed in the *F-C^N* (**2**, **5**, **8)** and the *CF_3-C^N* (**3**, **6**, **9**) series.

Likewise, changes in the HOMO energy are achieved by substitution at the *R* positions with F and CF_3 groups at each C^N ligand. For instance, with respect to **1**, the HOMO energy in the complexes **2** and **3** is decreased in 0.43 and 0.71 eV due to F and CF_3 substitutions, respectively. A similar behavior is evidenced when either the series containing the *R-pyz* (**4**-**6**) or the *R-pypy* ligand (**7-9**) are compared. The most stabilized HOMO levels (and the highest HL_{gap}) are found in systems containing CF_3; thus the CF_3 group appears to be a more electron-withdrawing group in comparison to fluorine in agreement with previous reports[31, 40].

According to the literature, the HOMO-LUMO modulation can be explained by means of mesomeric and inductive effects, among others[31]. The mesomeric effect relates to the sharing of the π electrons between the aromatic ligand and the substituent; this effect is low if the substituent is located at the position where the corresponding molecular orbital has nodes[31]. On the contrary, the inductive effects are associated with electron depletion in the σ-system by acceptor substituents; the latter induces a less repulsive Coulombic interaction between σ and π electrons in the cyclometalated ligand, and thus stabilizing the energy of the molecular orbital[31]. In this context, because of the HOMO in all of the complexes (Fig. 3) shows nodes at the positions 2 and 4 of the phenyl group (positions at which are added the *R* substituents), the stabilization of the HOMO energy would be influenced mainly due to the inductive effects. On the other hand, minor changes are found for the LUMO energy due to the N^N ligand is the same for all complexes.

Finally, the marked energy stabilization of the HOMO (in addition to the low LUMO stabilization) results in an enhancement of the HL_{gap}. In the case of the CF_3 containing complexes containing, the highest HL_{gap} are found with values of 3.15, 3.30 and 3.54 eV, for the complexes **3**, **6**, and **9**, respectively. The higher HL_{gap} of the complex **9** is consistent with the high acceptor nature of the cyclometalated ligands (according to the tendency *H-ppy<H-pyz<H-pypy*). It is important to note that the enhancement of the HL_{gap} is directly correlated to the photophysical properties of both excited and ground states. In this regard, the high stabilization of the HOMO level by use of CF_3 substituted ligands results in an enhancement of their HL_{gap}, which should result in blue-shifted electronic transitions either in the absorption or the emission processes. Since the luminescence at high energy is of great interest to obtain blue light in LEC devices, to include trifluoromethyl substituents for the modulation of the frontier molecular orbitals seems to be successful for the control of the luminescence process.

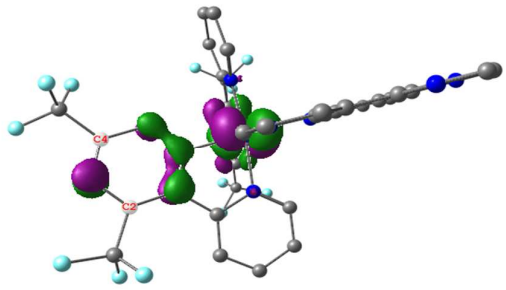

Fig. 3 HOMO of the complex **3** as representative of compounds **1**-**9**.

Absorption spectrum

At the TD-DFT level, the UV-Vis spectra of the complexes **1**-**9** were obtained in CH_2Cl_2 as solvent (excitation energies, oscillator strengths, monoexcitations and nature of the excited states are in Table S3 in the ESI†). We focused on the transitions at low energies, which are related to the optical properties of the cyclometalated Ir^{III} complexes, including phosphorescence and non-linear optics[7, 9, 41]. The latter is commonly related to the singlet metal-to-ligand charge transfer transitions (^{1}MLCT), but in Ir^{III} complexes these transitions are commonly mixed with singlet ligand-to-ligand charge transfer excitations (^{1}LLCT); note that these electronic transitions are responsible for the subsequent singlet-triplet intersystem crossing that controlled the emissive states[4].

In the complex **1**, the ^{1}MLCT transitions are located at 383 and 361 nm, in good agreement with the assignments of the experimental absorptions at 382 and 358 nm[23]. The transition at 383 nm is a mixed ^{1}MLCT/^{1}LLCT state; here the electron is promoted from the metal and C^N ligand toward the *H-ppl* ligand [Ir(d)+C^N(π)→ppl(π*)]. Moreover, a mainly ^{1}MLCT transition appears at 361 nm, where the electron is promoted toward the *H-ppl* ligand [Ir(d)→ppl(π*)]. Due to the fluorinated C^N ligands of **2** and **3**, the ^{1}MLCT/^{1}LLCT exited state appear shifted at high energies (~373 nm), due to the stabilization of the HOMO orbitals from which the transition is originated. The *H-pyz* and *H-pypy* ligands have an enhanced electron withdrawing character compared to *H-ppy*, thus the low energy ^{1}MLCT/^{1}LLCT transition appears blue-shifted at 373 and 361 nm for **4** and **7**, respectively, according to the description of the HL_{gap}; the absorption of complex 4 agree with their experimental bands between 370 and 380 nm[24].

In a similar way, the incorporation of F atoms in the C^N ligand enhances the blue-shifted transitions in the *R-pyz and R-pypy* based complexes (*R* = F or CF_3): the ^{1}MLCT/^{1}LLCT transition for **5** and **6** are located at 360 and 356 nm, respectively, while for **8** and **9** are located at 354 and 342 nm, respectively. Note that as expected, the enhanced blue shifts of the ^{1}MLCT excited states by the use of fluorinated C^N ligands in agreement with the stabilization of the HOMO levels and the trend in the HOMO-LUMO energy gap.

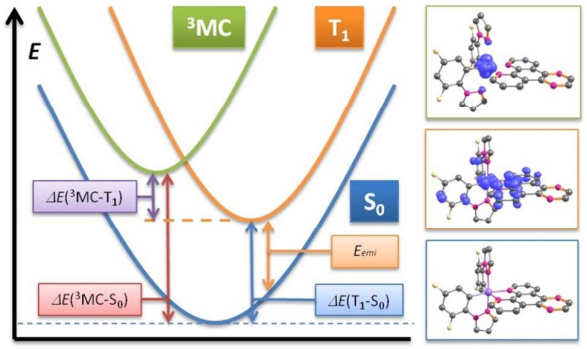

Fig. 4 Energy diagram showing the studied ground state (S0), first triplet excited states (T1) and metal centered state (3MC). Arrows depicts the main vertical energy differences: $\Delta E(^3MC\text{-}T_1)$, $\Delta E(^3MC\text{-}S_0)$, the 0-0 transitions energies [$\Delta E(T_1\text{-}S_0)$], and the emission energies (E_{emi}).

Luminescence properties

In this section we account for the luminescence properties of the complexes **1**-**9**. Fig. 4 shows the different deactivation pathways that can occur from the triplet excited states. Firstly, the emissive deactivation from the first triplet excited state (T_1) will be analyzed; in a second step, the possible non radiative processes coming from metal centered states (^{3}MC) are studied.

The emission energies in CH_2Cl_2 as solvent (E_{emi}) (Table 1) were obtained from the *ΔSCF* procedure, this is the vertical energy difference between the relaxed T_1 state and the S_0

Table 1 Properties of the T_1 excited state of complexes **1**-**9**: emission energies (E_{emi}, in eV) and wavelengths (λ_{emi}, in nm) in CH_2Cl_2 and gas phase; monoexcitations with weighting coefficients and percentage of contribution to the excited state wavefunction; and description of the electronic transition. H and L correspond to HOMO and LUMO, respectively.

system	E_{emi} $(\lambda_{emi})_{CH2Cl2}$	E_{emi} $(\lambda_{emi})_{gas\ phase}$	transitions	description
1	2.08 (597)	2.08 (595)	L→H (0.69)[95.59%]	ppl(π*)→Ir(d)+C^N(π); MLCT/LLCT
2	2.35 (528)	2.32 (534)	L→H (0.68)[93.44%]	ppl(π*)→Ir(d)+C^N(π); MLCT/LLCT
3	2.48 (501)	2.41 (514)	L→L (0.66)[88.37%]	ppl(π*)→Ir(d)+C^N(π); MLCT/LLCT
4	2.17 (572)	2.22 (559)	L→H (0.69)[96.31%]	ppl(π*)→Ir(d)+C^N(π); MLCT/LLCT
5	2.43 (510)	2.45 (505)	L→H (0.69)[95.81%]	ppl(π*)→Ir(d)+C^N(π); MLCT/LLCT
6	2.52 (492)	2.50 (496)	L→H-6 (-0.21)[8.97%]	ppl(π*)→ppl(π); LC
			L→H-1 (0.23)[10.89%]	ppl(π*)→Ir(d)+C^N(π); MLCT/LLCT
			L→H (0.60)[72.41%]	ppl(π*)→Ir(d)+C^N(π); MLCT/LLCT
7	2.54 (487)	2.48 (501)	L→H-9 (0.19)[7.59%]	ppl(π*)→ppl(π); LC
			L→H-4 (0.18)[6.71%]	ppl(π*)→Ir(d)+C^N(π); MLCT/LLCT
			L→H-2 (0.16)[5.07%]	ppl(π*)→Ir(d)+C^N(π); MLCT/LLCT
			L→H (0.60)[71.98%]	ppl(π*)→Ir(d)+C^N(π); MLCT/LLCT
8	2.79 (445)	2.69 (461)	L→H-6 (-0.37)[27.79%]	ppl(π*)→ppl(π); LC
			L→H-3 (0.42)[34.75%]	ppl(π*)→Ir(d); MLCT
			H→H (0.32)[20.20%]	ppl(π*)→Ir(d)+C^N(π); MLCT/LLCT
9	2.83 (438)	2.72 (456)	L→H-6 (0.38)[28.80%]	ppl(π*)→ ppl(π); LC
			L→H-2 (0.40)[31.64%]	ppl(π*)→Ir(d); MLCT
			L→H (-0.28)[15.42%]	ppl(π*)→Ir(d)+C^N(π); MLCT/LLCT

state at the T_1 state geometry (Fig. 4) (T_1 geometries compared to the ground states are in Table S1 of the ESI†). From Table 1, it is noted that the different unsubstituted ligands C^N perform different according as their electron-withdrawing character increases; complexes with the unsubstituted cyclometalating ligands *H-ppy* (**1**), *H-pyz* (**4**) and *H-pypy* (**7**) show emissions at 595, 559 and 501 nm, respectively; these values are consistent with experimental emission energies of 590 and 566 nm for complex **1** and **4**, respectively in CH_2Cl_2[23, 24]. Moreover, these findings are in agreement with the experimental properties of related cyclometalated Ir^{III} complexes, where the aromatic nature of the unsubstituted ligand induces changes on the photophysical properties of Ir^{III} complexes[17]. In this regard, studies of heteroleptic complexes of the type $[Ir(C^N)_2(N^N)]^+$ (where N^N is 1*H*-imidazo[4,5-*f*][1,10]phenanthroline and C^N is phenylpyridine or 1-phenylpyrazole) shows that the exchanging of phenylpyridine by phenylpyrazole induces a blue-shifted emission from 583 to 560 nm, attributable to the weaker σ-electron donor pyrazole group[40]. The modulation of the emission energy of related complexes, including indazole cyclometalating ligands was also studied; the use of N^N as 4,4´-ditertbutylpyridine and C^N as indazole derivative ligands, shows that the use of 1-phenylindazole or 2-phenyl-1,2,3-triazole as cyclometalating ligands shifts the emission bands from 575 to 520 nm[42, 43], in which displacement to higher energy is attributable to the electron withdrawing capability of the latter C^N moiety.

With respect to the substituents effect, a clear blue-shifted luminescence is caused by the fluorinated C^N ligands, even improved by use of the electrophilic CF_3 substitution. This is consistent with the emission energies obtained experimentally for related Ir^{III} complexes; for instance, in a series of homoleptic cyclometalated Ir^{III} complexes (including substituted phenylpiridine with fluorine atoms) the substitution (on the position 2 and 4 of phenylpiridine) induces an blue-shifted emission to 468 nm with respect to the emission at 510 nm of the unsubstituted complex[4]. Likewise, the effect of fluorination in heteroleptic bis-cyclometalated complexes of the type $[Ir(R_2ppy)_2(N^N)]^+$ (where N^N is 4,4´-dimethylaminopyridine and R_2ppy is phenylpyridine or 2,4-difluorophenylpyridine) afford a blue-shifted luminescence from 491 to 463 nm for the unsubstituted and the substituted complexes, respectively[4]. In addition, the CF_3 substitution on complexes of the type $[Ir(R\text{-}ppy)_2(N^N)]^+$ (where N^N is 4,7-diphenylphenanthroline and R-ppy is 4-fluorophenylpyridine or 4-trifluoromethylpyridine) results in a blue-shifted emission energy from 548 nm to 528 nm, attributable to the exchange of the fluorine by the CF_3 group[40]. In our case, the complexes **6**-**9** show emission energies in the range of 500-430 nm, with **9** showing the highest emission energy at 438 nm (2.83 eV). In summary, the values for emission energies follow the tend **1** < **4** < **2** < **5** < **3** < **6** < **7** < **8** < **9**; these values are in agreement with the decrease in the HL_{gap} with exception of the complexes **6**-**7**, although differences between them is only of ~5 nm. Moreover, the blue-shifted emission in the complexes **6**-**9** could be caused by mixing with of the ^{3}MLCT transitions with those of ^{3}LC (triplet ligand centered transition of the ancillary ligand) type, which will be discussed below. It is important to note that in Table 1 are also presented the values for emission energies in the gas phase; the latter data are included to explore the effect of the solvent polarization onto the emission energies, but the emission energies slightly change in a value of up to 0.11 eV, and then the complexes are able to retain the blue-shifted emission in comparison to compound **1**.

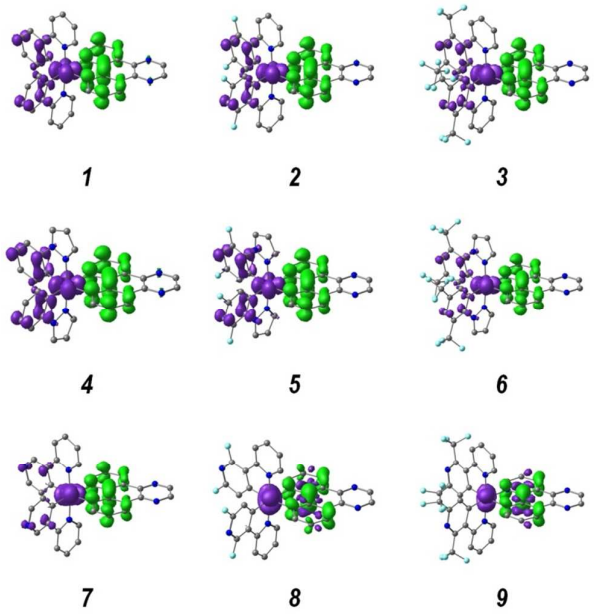

Fig. 5 Hole (green) and electron (purple) distributions for the deactivation of the first triplet excited state (T_1) state of complexes **1**-**9**. Hydrogen atoms were omitted in the molecular representation.

From the TD-DFT scheme, we account for the electronic transitions that are responsible for the radiative deactivation of the emissive states (Table 1). In addition, the hole-electron distributions are displayed in Fig. 5, which were obtained as:

$$\Delta\rho(r) = \rho^{electron}(r) - \rho^{hole}(r) \quad (1)$$

$$\rho^{hole}(r) = \sum_{i\to l}\left(w_i^l\right)^2\varphi_i(r)\varphi_i(r) + \sum_{i\to l}\sum_{j\neq i\to l} w_i^l w_j^l \varphi_i(r)\varphi_j(r) \quad (2)$$

$$\rho^{electron}(r) = \sum_{i\to l}(w_i^l)^2\varphi_i(r)\varphi_i(r) + \sum_{i\to l}\sum_{i\to m\neq l} w_i^l w_i^m \varphi_l(r)\varphi_m(r) \quad (3)$$

where ρ^{hole} and $\rho^{electron}$ are the density distributions of hole and electron in a given excited state wavefunction, respectively; w is the weighting coefficient of each monoexcitations due to promotion of one electron from the occupied orbital i to the virtual orbital j; φ stands for the occupied (or virtual) molecular orbital. An extensive derivation of the formulation can be found in the Multiwfn program[35]. In

the complexes **1-5**, the lowest triplet excited state (T_1) is mainly deactivated by a LUMO→HOMO transition (>88 %) of mixed ^{3}MLCT/^{3}LLCT character [ppl(π*)→Ir(d)+C^N(π)], thus these ones imply charge transfer from the ancillary ligand toward the metal and C^N ligand (Fig. 5). Note that we use the ^{3}MLCT term to characterize the T_1 state, although the reader must interpret that a ligand-to-metal charge transfer occurs in the deactivation process; the latter is used to be in agree with the literature discussions[44]. In the complexes **6**-**7**, the contribution of the LUMO→HOMO transition to the radiative processes is decreased up to 72 %; the deactivation pathway has a slight contribution of ligand centered (^{3}LC) π*→π transitions (~8-9 %), which are centered in the N^N ppl ligand. The ^{3}LC state of the ppy ligand was computed to 3.14 eV above its ground state; taking into account that **7**-**9** shows their T_1 states at least 2.90 eV above their ground states, a mixing with the nearing ^{3}LC state of the ppl ligand can be expected in these cases as noted below. Indeed, the complexes **8-9** shows an increased multiconfigurational character of the T_1 state, which is composed by several monoexcitations contributing with higher coefficients to the excited state wavefunction, thus the deactivation is not only due to LUMO→HOMO transitions (which contributes only up to ~20 %). The strong blue-shifted emission in these complexes is associated with the contribution of high-energy transitions, such as the π→π*, in agreement with the ^{3}LC contributions to the T_1 state[4]. In **8-9**, the ^{3}LC character of the T_1 state increase up to ~28 % and the excited state is correctly assigned as mixed contributions coming mainly from ^{3}MLCT and ^{3}LC. The latter implies that the deactivation of the T_1 state of the complexes **8-9** occurs mainly by charge transfer from the ppl fragment toward the metal core and the ppl fragment, as can be noted from the hole-electron distribution (Fig. 5). Moreover, the increased multiconfigurational character of the T_1 state in the complexes **8**-**9** is associated to its proximity to high excited states as was observed for related Ir^{III} complexes[33].

On the other hand, the phosphorescence quantum efficiency (Φ_p) is related to the radiative rate constant by the equation $\Phi_p=k_r/(k_r+k_{nr})$, where k_r and k_{nr} are the radiative and non-radiative rate constants, respectively. This implies that the competition between k_r and k_{nr} determine the performance of the phosphorescence. The Energy Gap Law establish that the emission energy is inversely proportional to ln(k_{nr}); therefore, the blue emitters are related to higher Φ_p values[18, 19, 45], resulting in an enhanced luminescence performance of the emitter compounds. Even so, the last assumption avoids the deactivation coming from thermally accessible states like the metal centered d→d transitions, which can be obtained by crossing between the different potential energy surfaces of the triplet excited states. As depicted in Fig. 4, the population of the metal centered triplet excited states (^{3}MC) results in a deactivation pathway of the emitting T_1 state in transition metal complexes[46-49]. These non-radiative excited states result from thermal activation, and they involve electron promotion from the occupied t_{2g} orbitals toward the unoccupied e_g orbitals of the metal core.

To analyze the possible deactivation processes coming from thermally accessible excited states, we obtained the optimized geometries of all the complexes in their ^{3}MC states by distorting the T_1 geometry in the ligand-metal region. The e_g orbital of the ^{3}MC state has an σ-antibonding character, thus the main structural change expected to take place is an increase of the distance Ir-N$_{(C^N)}$ and Ir-N$_{ppl}$. Indeed, partial decoordination is observed for all the complexes (geometrical parameters are in Table S5 of the ESI†); the Ir-N$_{(C^N)}$ bond lengths reach values in the range of 2.58 - 2.45 Å, which increases to ~ 0.5 Å with respect to the S_0 state. The Ir-N$_{ppl}$ bonds elongate up to ~ 0.1 Å, with the bond lengths in the range of 2.29 - 2.21 Å. The Ir-C(C^N) bond remains almost unchanged and ranges between 2.03-2.00 Å. Fig. 6 shows as the non-radiative deactivation involves electron transfer between the excited e_g orbital and the t_{2g} orbital for the complexes **1**, **4**, and **7** (the trend is similar along all the compounds).

The adiabatic energy difference between the T_1 and ^{3}MC states [ΔE(^{3}MC-T_1)] were analyzed as a measure of the accessibility to the radiationless processes (Table 2). Although, Ir^{III} based complexes have higher metal-centered d-d

Fig. 6 e_g and t_{2g} orbitals involved in the non-radiative d→d transitions from the ^{3}MC state toward S_0 state for complexes **1**, **4**, and **7** as representatives.

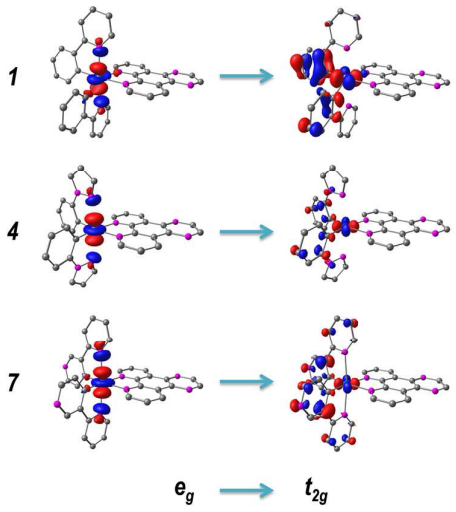

Table 2. Vertical energy differences as depicted in Figure 3: ΔE(^{3}MC-T_1), ΔE(^{3}MC-S_0), the adiabatic 0-0 transitions energies [ΔE(T_1-S_0)], and the emission energies (E_{emi}). Values in eV, and computed in CH_2Cl_2 as solvent.

system	ΔE(^{3}MC-T_1)	ΔE(^{3}MC-S_0)	ΔE(T_1-S_0)	E_{emi}
1	0.61	2.76	2.15	2.08
2	0.42	2.84	2.42	2.35
3	0.24	2.80	2.56	2.48
4	0.42	2.67	2.25	2.17
5	0.33	2.84	2.52	2.43
6	0.12	2.76	2.64	2.52
7	0.29	2.90	2.62	2.54
8	0.14	2.98	2.84	2.79
9	0.03	2.93	2.90	2.83

transitions compared to other emitters[5, 50], the $\Delta E(^3MC\text{-}T_1)$ value have been shown to play an important role in the luminescence performance of complexes tested in LEC devices[49, 51]. We found that all the optimized ^3MC states remain above the T_1 state, and the $\Delta E(^3MC\text{-}T_1)$ energy can be related to the computed emission energies as noted below. Complexes showing emission above 550 nm (**1** and **4**) have the ^3MC states at least 0.42 eV above the T_1 state, and therefore these must result in a more efficient phosphorescence emitters. In addition, complexes **2**, **4**, and **7** show $\Delta E(^3MC\text{-}T_1)$ values in the range of 0.24-0.33 eV. In this regard, Costa and co-workers reported $\Delta E(^3MC\text{-}T_1)$ values on the range of 0.26 to 0.60eV for related Ir^{III} complexes, which have shown luminance of 70 to 110 cd/m^2 in LECs[51]. According to this comparison, the complexes with $\Delta E(^3MC\text{-}T_1)$ values on the order of 0.20-0.60 eV are expected to show both good luminance performances and living times of the device. Indeed, we recently measure the performance of the complex **2** in a LEC device[20], which has shown a luminance value of ~177 cd/m^2. On the contrary, the blue emitters **6**, **8**, and **9** show low $\Delta E(^3MC\text{-}T_1)$ values of until 0.14 eV above the T_1 state, which would result in more accessible non-radiative states, decreased luminescence efficiency and lower living times that must be take into account in the effort for the synthesis of these compounds.

These results can be understood in terms of that the increasing of the electron-withdrawing character of the C^N ligand allows the blue-shifted luminescence, but also increasing the T_1 state energy. Additionally, the larger multiconfigurational character of these states allows the mixing with high excited states as was previously noted. In this regard, the 0-0 transition energies $\Delta E(T_1\text{-}S_0)$ (this is the electronic transition between the lowest vibrational modes of the ground singlet and triplet state, Fig. 4) show that the increase of the T_1 energy (respect to the ground state) is largely affected by the modification of the ligand compared to those found for the ^3MC states [$\Delta E(^3MC\text{-}S_0)$]. Indeed, the $\Delta E(^3MC\text{-}S_0)$ values increase only up to 0.17 eV, in comparison with the $\Delta E(T_1\text{-}S_0)$ values with an increase of up to 0.41 eV, thus causing low $\Delta E(^3MC\text{-}T_1)$ values as the electron-withdrawing effects increase. Note that the decreased performance of photoluminescence predicted from the adiabatic energy difference between the $^3MC\text{-}T_1$ states requires of experimental temperature-dependent analysis in order to achieve the activation energy barriers for the population of the ^3MC states; however, it is important to note that access to the ^3MC states can be avoided by a restricted intramolecular motion of the stretching vibrations of the Ir-ligand bonds[5]. In this regard, the temperature dependent analysis shows that the energy barrier for non radiative decays is increased ~80 % by using polymeric films as guest materials for the iTMCs compared to measurements in solution[52].

Finally, although a direct correlation between the emission energies and the quantum yields is commonly established by the energy gap law, a quantitative relation with the structural properties of the systems becomes sometimes more difficult to correlate. However, regarding the differences between the structural parameters of the ^3MC and T_1 states (Table S1 and S5), we observe that the larger geometric differences are found in the complexes **1-6**, mainly by comparing the angles and dihedrals associated with the octahedral coordination center. For instance, the most distorted ∠N1-Ir-N2 angle is found in the complexes **1-3,** with a difference of at least 16° between the ^3MC and T_1 geometries. On the contrary, the systems **7-9** show a less distortion of up to 4° between the ^3MC and T_1 states. At least, these results seem to be in qualitative agreement with the $\Delta E(^3MC\text{-}T_1)$ values; this is, large distortions cause higher energy differences, avoiding the probability of radiationless decaying.

system	IP	EA	λ_{hole}	$\lambda_{electron}$
1	8.95	3.70	0.18	0.35
2	9.38	3.89	0.16	0.36
3	9.61	4.06	0.19	0.35
4	9.15	3.70	0.20	0.35
5	9.57	3.90	0.20	0.36
6	9.83	4.04	0.27	0.39
7	9.65	3.92	0.17	0.36
8	10.06	4.11	0.14	0.37
9	10.22	4.26	0.16	0.35

Table 3. Electronic parameters related to transport and injection: Ionization potential (*IP*), electron affinity (*EA*), and reorganization energies (λ_{hole} and $\lambda_{electron}$). Energies are in electron-volt (eV).

Electron affinity and ionization potential

The working mechanism of LEC devices can be explained in the basis of an electrochemical doping model[53-56], where the formation of highly conductive p- and n-doped regions is accomplished by the displacement of ions at the anode and cathode, in the device. In the n-doped region the electrons are added from cathode, and holes are injected in the p-doped zone from anode. Under the application of the bias, these regions begin to widen until the hole-electron recombination takes place, promoting the emission of light[53-56]. According to some studies, the performance of Ir^{III} complexes in emitting devices can be related to several electronic properties evaluating the charge transport and electron (hole) injection[30, 32]. Indeed, the hole and electron injection ability of the iTMCs play an important role in the luminance and lifetime, limiting the current density in the device; in this case, a low charge transport is responsible for the poor LEC performance[57]. In this context, the thermodynamic parameters relating to the ionization potential (*IP*) and electron affinity (*EA*), account for the energy barrier for the hole and electron injection, respectively. Theoretical studies have related the easier hole injection from the anode into the emissive compound to a small *IP*, while a larger *EA* is related to the easy electron injection from the cathode[30, 32, 58]. This description is coherent with a good performance of the device due to the low turn-on voltage[20]. *IP* and *EA* values for all the complexes were obtained by finite difference as $IP = E(N-1) - E(N)$ and $EA = E(N) - E(N+1)$; where $E(N)$, $E(N+1)$ and $E(N-1)$ are

the total energies of the molecular system in its ground state, and with one electron more and with one electron less, respectively.

From Table 3, it is noted that the smallest *IP* is obtained for the system **1**, resulting in an easier hole injection compared to the other complexes, according to its higher HOMO energy level compared to the complexes **2**-**9**. The easily for the hole injection from the anode is sorted as: **1** > **4** > **2** > **5** > **3** > **7** > **6** > **8** > **9**, following a similar order to the HOMO energies. On the contrary, differences in the *EA* values of the all complexes are slightly compared with the *IP* values. This behavior is attributed to the nature of the same ppl ancillary ligand in all complexes and also in accordance with the simulation of the LEC performance described in literature. This performance establish that an easy electron injection is not as decisive as the barrier which determines the hole injection[53]. In this sense, it is possible to conclude that the similar *EA* values for all the compounds is an indicative that the hole-electron recombination of the LEC devices with these complexes is controlled mainly by the *IP* of the compounds.

The high *EA* is obtained from the complex **9**, and the lowest energy barrier for electron injection into the emitter is also expected for this compound, which is consistent with its lower LUMO energy compared to **1**-**8**. The same relationship of the *IP* with the HOMO energies is feasible with the tendency of the *EA* values and LUMO energies. The *EA* values have the following order: **9 > 8 > 3 > 6 > 7 > 5 > 2 > 4 > 1**. We note a balance between the hole and electron injection properties of the emitter for the complexes in the middle of the series (**2**-**3** and **5**-**7**), highlighting the complex **7** to develop a better hole-electron junction.

On the other hand, the reorganization energies for hole and electron transport (λ_{hole} and $\lambda_{electron}$) are related to the charge transfer rate (*k*) according to $k=Aexp(-\lambda/k_bT)$: where k_b is the Boltzmann constant, and *T* the temperature[30, 32, 58]. These kinetic parameters are obtained as: $\lambda_{hole} = IP - HEP$ and $\lambda_{electron} = EA - EEP$, where *HEP* and *EEP* are the so-called hole and electron extraction potential, respectively. The magnitude of *HEP* and *EEP* are obtained as the *ΔSCF* energy difference between the relaxed cationic (anionic) molecule and the neutral molecule at the cationic (anionic) geometry[30]. We pointed from Table 3 that the reorganization energies for the electron transport ($\lambda_{electron}$) are higher compared to those for the hole transport (λ_{hole}), which is mainly due to the cationic nature of the complexes. These results suggest that the performance of the complexes for hole transport is better than for the electron transport. The smallest λ_{hole} was found for the complex **8**, suggesting an improved hole transport in this compound. Moreover, $\lambda_{electron}$ values are very similar for all the complexes, indicating a similar electron transport rate between all the complexes. However, the difference between λ_{hole} and $\lambda_{electron}$ is smallest for the complex **6**, suggesting a charge transport balance between hole and electron injection for this compound, which can be useful to improve the hole (electron) transfer abilities in electroluminescent devices based in cationic Ir complexes.

Conclusions

In summary, a theoretical characterization of nine cationic Ir^{III} complexes $[Ir(C^N)_2(N^N)]^+$ was performed to get insights about their applicability as ionic transition metal complexes for light electrochemical cells (LECs). All of these complexes contain the *ppl* ancillary ligand (N^N), and the control onto the HOMO energy was reached by changing the cyclometalating C^N ligands (*R-ppy*, *R-pyz* and *R-pypy*); however, both HOMO and LUMO energy levels appear to be influenced by the nature of the unsubstituted cyclometalating ligands (with *R* = H), in addition to inductive effects coming from electron-withdrawing fluorine containing substituents (*R* = F, CF_3) at the 2 and 4 positions of the phenyl moiety. In consequence, HOMO-LUMO energy gaps were found in the range of 2.76 to 3.54 eV, and phosphorescence emission energies in the range of 438 to 597 nm; the highest HOMO-LUMO energy gap and blue-shifted emission (and absorption) energies were obtained for the complexes containing the trifluoromethyl substituents in the cyclometalating ligand. The emission energies are modulated due to metal-to-ligand charge transfer triplet excited states; however, the strong blue-shifting in compounds containing the *CF_3-pyz*, *F-pypy* and *CF_3-pypy* ligands (complexes **6**, **8**, and **9**, respectively) is accompanied by mixing with ligand and metal centered triplet states, also responsible for a decreased photoluminescence performance. Respect to transport and injection parameters, the complexes with the best balance between hole and electron injection are **2**, **3**, **5**, **6** and **7**; however, as all complexes have the same ancillary ligand, the different performances are controlled mainly by the ionization potential of the complexes. In the same way, according to the reorganization energies, the energies for the electron transport ($\lambda_{electron}$) are higher compared to those for the hole transport (λ_{hole}), which is attributed to the cationic nature of the complexes; then, the performance of the complexes for hole transport is better that for the electron transport. The smallest λ_{hole} was found for complex **8**. However, the difference between λ_{hole} and $\lambda_{electron}$ is smallest for the complex **6**, therefore, this complex show the best balance between hole-electron junctions.

Acknowledgements

This work was supported by ICM grant N°120082 and FONDECYT N°1130072. D.C.A acknowledges to FONDECYT/Postdoctorado N°3140314. P.D. acknowledges to FONDECYT Project 11130221 and USM-Project 131439.

Notes and References

1. M. Baldo, S. Lamansky, P. Burrows, M. Thompson and S. Forrest, *Appl. Phys. Lett.*, 1999, **75**, 4.
2. A. B. Tamayo, B. D. Alleyne, P. I. Djurovich, S. Lamansky, I. Tsyba, N. N. Ho, R. Bau and M. E. Thompson, *J. Am. Chem. Soc.*, 2003, **125**, 7377-7387.

3. S. Huo, J. C. Deaton, M. Rajeswaran and W. C. Lenhart, *Inorg. Chem.*, 2006, **45**, 3155-3157.
4. E. Baranoff, J.-H. Yum, M. Graetzel and M. K. Nazeeruddin, *J. Organomet. Chem.*, 2009, **694**, 2661-2670.
5. Y. You and S. Y. Park, *Dalton Trans.*, 2009, 1267-1282.
6. S. Lamansky, P. Djurovich, D. Murphy, F. Abdel-Razzaq, H.-E. Lee, C. Adachi, P. E. Burrows, S. R. Forrest and M. E. Thompson, *J. Am. Chem. Soc.*, 2001, **123**, 4304-4312.
7. V. Aubert, L. Ordronneau, M. Escadeillas, J. G. Williams, A. Boucekkine, E. Coulaud, C. Dragonetti, S. Righetto, D. Roberto and R. Ugo, *Inorg. Chem.*, 2011, **50**, 5027-5038.
8. K. P. S. Zanoni, R. L. Coppo, R. C. Amaral and N. Y. M. Iha, *Dalton Trans.*, 2015, **44**, 14559-14573.
9. S. Fantacci and F. De Angelis, *Coord. Chem. Rev.*, 2011, **255**, 2704-2726.
10. M. S. Lowry, J. I. Goldsmith, J. D. Slinker, R. Rohl, R. A. Pascal, G. G. Malliaras and S. Bernhard, *Chem. Mater.*, 2005, **17**, 5712-5719.
11. R. D. Costa, E. Ortí, H. J. Bolink, F. Monti, G. Accorsi and N. Armaroli, *Angew. Chem., Int. Ed.*, 2012, **51**, 8178-8211.
12. T. Hu, L. He, L. Duan and Y. Qiu, *J. Mater. Chem.*, 2012, **22**, 4206-4215.
13. P. L. Feng, J. Villone, K. Hattar, S. Mrowka, B. M. Wong, M. D. Allendorf and F. P. Doty, *IEEE Trans. Nuclear Sci.*, 2012, **59**, 3312-3319.
14. I. Campbell and B. Crone, *Appl. Phys. Lett.*, 2007, **90**, 012117.
15. C.-J. Yang, T.-Y. Cho, C.-L. Lin and C.-C. Wu, *Appl. Phys. Lett.*, 2007, **90**, 173507.
16. V. K. Khanna, *Fundamentals of Solid-state Lighting: LEDs, OLEDs, and Their Applications in Illumination and Displays*, CRC Press, 2014.
17. V. Balzani, S. Campagna and A. Barbieri, *Photochemistry and Photophysics of Coordination Compounds II*, Springer-Verlag Berlin Heidelberg, 2007.
18. M. Arias, J. Concepción, I. Crivelli, A. Delgadillo, R. Díaz, A. Francois, F. Gajardo, R. López, A. M. Leiva and B. Loeb, *Chem. Phys.*, 2006, **326**, 54-70.
19. G. F. Strouse, J. R. Schoonover, R. Duesing, S. Boyde, W. E. J. Jones and T. J. Meyer, *Inorg. Chem.*, 1995, **34**, 473-487.
20. I. González, P. Dreyse, D. Cortés-Arriagada, M. Sundararajan, C. Morgado, I. Brito, C. Roldán-Carmona, H. J. Bolink and B. Loeb, *Dalton Trans.*, 2015, **44**, 14771-14781.
21. M. S. Lowry and S. Bernhard, *Chem. - Eur. J.*, 2006, **12**, 7970-7977.
22. J. D. Slinker, J. Rivnay, J. S. Moskowitz, J. B. Parker, S. Bernhard, H. D. Abruña and G. G. Malliaras, *J. Mater. Chem.*, 2007, **17**, 2976-2988.
23. K. K. W. Lo, C. K. Chung and N. Zhu, *Chem. - Eur. J.*, 2006, **12**, 1500-1512.
24. K. Y. Zhang, S. P.-Y. Li, N. Zhu, I. W.-S. Or, M. S.-H. Cheung, Y.-W. Lam and K. K.-W. Lo, *Inorg. Chem.*, 2010, **49**, 2530-2540.
25. M. J. Frisch, G. W. Trucks, H. B. Schlegel, G. E. Scuseria, M. A. Robb, J. R. Cheeseman, G. Scalmani, V. Barone, B. Mennucci, G. A. Petersson, H. Nakatsuji, M. Caricato, X. Li, H. P. Hratchian, A. F. Izmaylov, J. Bloino, G. Zheng, J. L. Sonnenberg, M. Hada, M. Ehara, K. Toyota, R. Fukuda, J. Hasegawa, M. Ishida, T. Nakajima, Y. Honda, O. Kitao, H. Nakai, T. Vreven, J. A. Montgomery, J. E. Peralta, F. Ogliaro, M. Bearpark, J. J. Heyd, E. Brothers, K. N. Kudin, V. N. Staroverov, R. Kobayashi, J. Normand, K. Raghavachari, A. Rendell, J. C. Burant, S. S. Iyengar, J. Tomasi, M. Cossi, N. Rega, J. M. Millam, M. Klene, J. E. Knox, J. B. Cross, V. Bakken, C. Adamo, J. Jaramillo, R. Gomperts, R. E. Stratmann, O. Yazyev, A. J. Austin, R. Cammi, C. Pomelli, J. W. Ochterski, R. L. Martin, K. Morokuma, V. G. Zakrzewski, G. A. Voth, P. Salvador, J. J. Dannenberg, S. Dapprich, A. D. Daniels, Farkas, J. B. Foresman, J. V. Ortiz, J. Cioslowski and D. J. Fox, *Gaussian 09*, Rev. B.01, Wallingford CT.
26. A. D. Becke, *J. Chem. Phys.*, 1993, **98**, 5648-5652.
27. W. J. Hehre, R. Ditchfield and J. A. Pople, *J. Chem. Phys.*, 1972, **56**, 2257-2261.
28. M. M. Francl, W. J. Pietro, W. J. Hehre, J. S. Binkley, M. S. Gordon, D. J. DeFrees and J. A. Pople, *J. Chem. Phys.*, 1982, **77**, 3654-3665.
29. P. J. Hay and W. R. Wadt, *J. Chem. Phys.*, 1985, **82**, 299-310.
30. X.-N. Li, Z.-J. Wu, Z.-J. Si, H.-J. Zhang, L. Zhou and X.-J. Liu, *Inorg. Chem.*, 2009, **48**, 7740-7749.
31. I. Avilov, P. Minoofar, J. Cornil and L. De Cola, *J. Am. Chem. Soc.*, 2007, **129**, 8247-8258.
32. D. Han, F. Hao, J. Tian, C. Pang, J. Li, L. Zhao and G. Zhang, *J. Lumin.*, 2015, **159**, 66-72.
33. P. Pla, J. M. Junquera-Hernández, H. J. Bolink and E. Ortí, *Dalton Trans.*, 2015, **44**, 8497-8505.
34. J. M. Younker and K. D. Dobbs, *J. Phys. Chem. C*, 2013, **117**, 25714-25723.
35. T. Lu and F. Chen, *J. Comput. Chem.*, 2012, **33**, 580-592.
36. X. Zeng, M. Tavasli, I. F. Perepichka, A. S. Batsanov, M. R. Bryce, C. J. Chiang, C. Rothe and A. P. Monkman, *Chem. - Eur. J.*, 2008, **14**, 933-943.
37. F. Monti, A. Baschieri, I. Gualandi, J. J. Serrano-Pérez, J. M. Junquera-Hernández, D. Tonelli, A. Mazzanti, S. Muzzioli, S. Stagni and C. Roldan-Carmona, *Inorg. Chem.*, 2014, **53**, 7709-7721.
38. R. D. Costa, E. Ortí, H. J. Bolink, S. Graber, S. Schaffner, M. Neuburger, C. E. Housecroft and E. C. Constable, *Adv. Funct. Mater.*, 2009, **19**, 3456-3463.
39. L. Flamigni, A. Barbieri, C. Sabatini, B. Ventura and F. Barigelletti, in *Photochemistry and Photophysics of Coordination Compounds II*, Springer, 2007, pp. 143-203.
40. N. M. Shavaleev, R. Scopelliti, M. Grätzel and M. K. Nazeeruddin, *Inorg. Chim. Acta*, 2013, **396**, 17-20.
41. Y. You and W. Nam, *Chem. Soc. Rev.*, 2012, **41**, 7061-7084.
42. N. M. Shavaleev, R. Scopelliti, M. Grätzel and M. K. Nazeeruddin, *Inorg. Chim. Acta*, 2012, **388**, 84-87.

43. N. M. Shavaleev, R. Scopelliti, E. Baranoff, M. Grätzel and M. K. Nazeeruddin, *Inorg. Chim. Acta*, 2012, **383**, 316-319.
44. D. Tordera, M. Delgado, E. Ortí, H. J. Bolink, J. Frey, M. K. Nazeeruddin and E. Baranoff, *Chem. Mater.*, 2012, **24**, 1896-1903.
45. R. Englman and J. Jortner, *Mol. Phys.*, 1970, **18**, 145-164.
46. F. Kessler, R. D. Costa, D. Di Censo, R. Scopelliti, E. Ortí, H. J. Bolink, S. Meier, W. Sarfert, M. Grätzel and M. K. Nazeeruddin, *Dalton Trans.*, 2012, **41**, 180-191.
47. T. Sajoto, P. I. Djurovich, A. B. Tamayo, J. Oxgaard, W. A. Goddard III and M. E. Thompson, *J. Am. Chem. Soc.*, 2009, **131**, 9813-9822.
48. F. Alary, J.-L. Heully, L. Bijeire and P. Vicendo, *Inorg. Chem.*, 2007, **46**, 3154-3165.
49. R. D. Costa, F. Monti, G. Accorsi, A. Barbieri, H. J. Bolink, E. Ortí and N. Armaroli, *Inorg. Chem.*, 2011, **50**, 7229-7238.
50. K. Dedeian, J. Shi, E. Forsythe, D. C. Morton and P. Y. Zavalij, *Inorg. Chem.*, 2007, **46**, 1603-1611.
51. R. D. Costa, E. Ortí, H. J. Bolink, S. Graber, C. E. Housecroft, M. Neuburger, S. Schaffner and E. C. Constable, *Chem. Commun.*, 2009, 2029-2031.
52. R. E. Harding, S.-C. Lo, P. L. Burn and I. D. W. Samuel, *Org. Electron.*, 2008, **9**, 377-384.
53. J. D. Slinker, J. A. DeFranco, M. J. Jaquith, W. R. Silveira, Y.-W. Zhong, J. M. Moran-Mirabal, H. G. Craighead, H. D. Abruna, J. A. Marohn and G. G. Malliaras, *Nat. Mater.*, 2007, **6**, 894-899.
54. Q. Pei, G. Yu, C. Zhang, Y. Yang and A. J. Heeger, *Science*, 1995, **269**, 1086-1088.
55. Q. Pei, Y. Yang, G. Yu, C. Zhang and A. J. Heeger, *J. Am. Chem. Soc.*, 1996, **118**, 3922-3929.
56. D. Smith, *J. Appl. Phys.*, 1997, **81**, 2869-2880.
57. A. M. Bünzli, H. J. Bolink, E. C. Constable, C. E. Housecroft, J. M. Junquera-Hernández, M. Neuburger, E. Ortí, A. Pertegás, J. J. Serrano-Pérez and D. Tordera, *Dalton Trans.*, 2014, **43**, 738-750.
58. D. Han, X. Shang, L. Zhao, X. Sun, G. Zhang and W. Ji, *Mol. Phys.*, 2014, **112**, 1824-1830.

